Cl-Doped ZnO Nanowire Arrays on 3D Graphene Foam with Highly Efficient Field Emission and Photocatalytic Properties

Dali Shao, Jian Gao, Guoqing Xin, Yiping Wang, Lu Li, Jian Shi, Jie Lian, Nikhil Koratkar,* and Shayla Sawyer**

***A**n environmentally friendly, low-cost, and large-scale method is developed for fabrication of Cl-doped ZnO nanowire arrays (NWAs) on 3D graphene foam (Cl-ZnO NWAs/GF), and investigates its applications as a highly efficient field emitter and photocatalyst. The introduction of Cl-dopant in ZnO increases free electrons in the conduction band of ZnO and also leads to the rough surface of ZnO NWAs, which greatly improves the field emission properties of the Cl-ZnO NWAs/GF. The Cl-ZnO NWAs/GF demonstrates a low turn-on field (≈1.6 V μm^{-1}), a high field enhancement factor (≈12844), and excellent field emission stability. Also, the Cl-ZnO NWAs/GF shows high photocatalytic efficiency under UV irradiation, enabling photodegradation of organic dyes such as RhB within ≈75 min, with excellent recyclability. The excellent photocatalytic performance of the Cl-ZnO NWAs/GF originates from the highly efficient charge separation efficiency at the heterointerface of Cl-ZnO and GF, as well as improved electron transport efficiency due to the doping of Cl. These results open up new possibilities of using Cl-ZnO and graphene-based hybrid nanostructures for various functional devices.*

Dr. D. Shao, Prof. S. Sawyer
Department of Electrical
Computer, and Systems Engineering
Rensselaer Polytechnic Institute
Troy, NY 12180, USA
E-mail: sawyes@rpi.edu

J. Gao, Y. Wang, Prof. J. Shi, Prof. N. Koratkar
Department of Materials Science and Engineering
Rensselaer Polytechnic Institute
Troy, NY 12180, USA
E-mail: koratn@rpi.edu

G. Xin, L. Li, Prof. J. Lian, Prof. N. Koratkar
Department of Mechanical
Aerospace and Nuclear Engineering
Rensselaer Polytechnic Institute
Troy, NY 12180, USA
E-mail: lianj@rpi.edu

DOI: 10.1002/smll.201501411

1. Introduction

As a wide bandgap semiconductor, ZnO has drawn significant research interest due to its unique optical and electrical properties including large exciton binding energy (60 meV) at room temperature, low electron affinity, high thermal stability, and environmental friendliness.[1–3] Furthermore, the easy fabrication of ZnO-based nanostructures with various shapes has made them attractive building blocks for a wide variety of nanodevices.[4–6] In particular, ZnO nanostructures have been investigated for fabrication of high-quality field emitters, which have important applications in flat-panel displays, microwave amplifiers, parallel-electron-beam microscopes, and X-ray radiotherapy, etc.[7] Recently, many efforts have been employed to enhance the field-emission properties of various ZnO-based nanostructures such as control of

morphology,[8] doping with selective elements,[9,10] plasma treatment,[11] coating with amorphous carbon or carbon nitride films,[12] and thermal annealing.[13] An emerging new concept is to grow ZnO nanostructures on highly conductive substrates to be used as negative electrodes for field emission, a design that has several apparent advantages including reduced barrier resistance between the material and the substrate, and renders other auxiliary components like conductive agents and binders completely unnecessary in conventional thin-film electrodes.[14] Graphene, as a novel carbon nanomaterial, has many superior material properties including high carrier transport mobility, large specific surface area, superior mechanical properties, and excellent chemical stability.[15–17] Therefore, growth of ZnO nanostructures on graphene-based substrates would be a promising strategy to boost the performance of ZnO-based field emitters. Moreover, there has been significant research activity devoted to the development of various graphene–semiconductor composite photocatalyst due to their significantly improved photocatalytic efficiency.[18–24] The ZnO–graphene heterointerfaces can greatly facilitate the separation of photogenerated electron-hole pairs in ZnO, making ZnO–graphene hybrid nanostructures also promising for other applications such as photosensing, photocatalysis, and water splitting.[25–27]

In this contribution, we developed an environmentally friendly, low-cost, and large-scale synthetic method for growth of closely packed and aligned Cl-doped ZnO nanowire arrays (NWAs) on 3D graphene foam (Cl-ZnO NWAs/GF). The 3D graphene foam has a large specific surface area, which enables the growth of large amount of ZnO NWs as emission spots. In addition, using graphene foam as a conductive substrate can significantly improve the carrier transport/separation efficiency of the hybrid material system, which is favorable for field emission and photocatalyst applications. Our experiments demonstrated superior field emission properties and high photocatalytic efficiency for the Cl-ZnO NWAs/GF. To the best of our knowledge, this is the first report that systematically investigates the field emission and photocatalytic properties of Cl doped ZnO NWs grown on GF.

2. Results and Discussion

2.1. Material Characterization

The scanning electron microscope (SEM) images of the as-synthesized graphene foam are shown in **Figure 1**a,b.

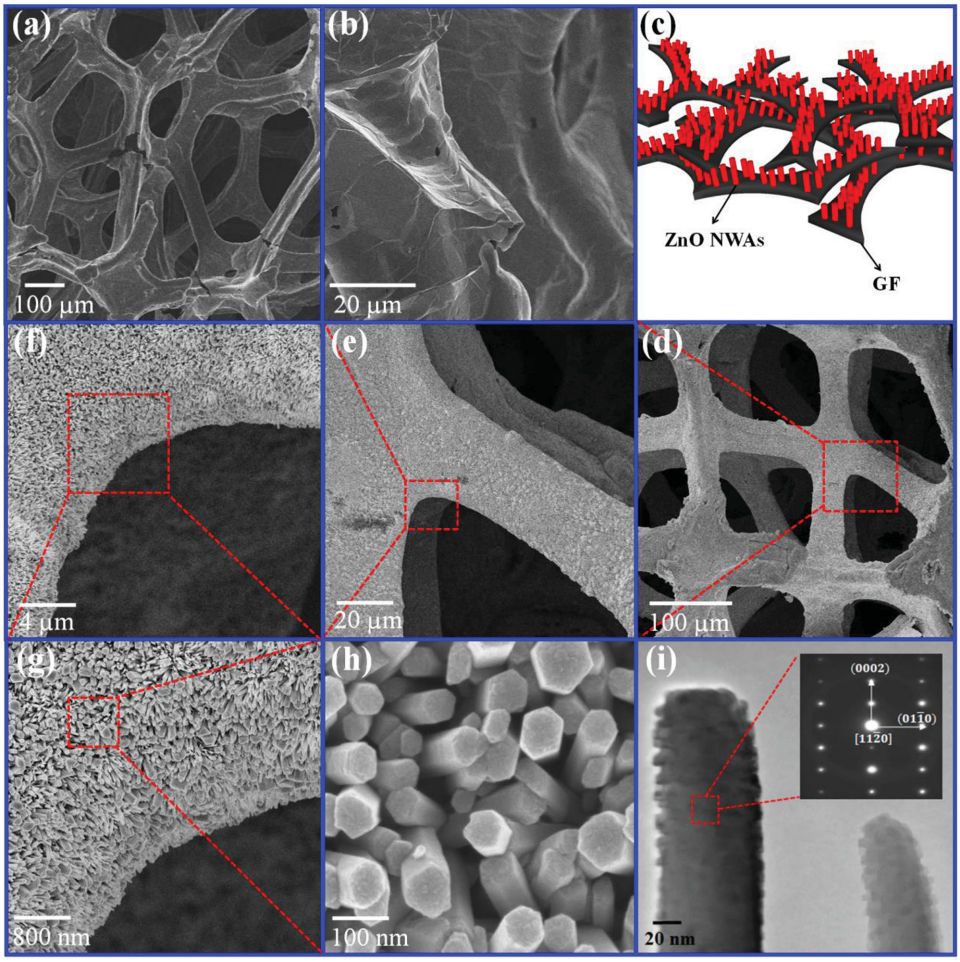

Figure 1. a,b) SEM images of 3D GF at different magnifications. c) Schematic illustration of the Cl-ZnO NWAs/GF. d–h) SEM images of the Cl-ZnO NWAs on the 3D GF at different magnifications. i) TEM image of the Cl-ZnO NWAs on 3D GF, the inset shows the diffraction pattern of the ZnO NWAs.

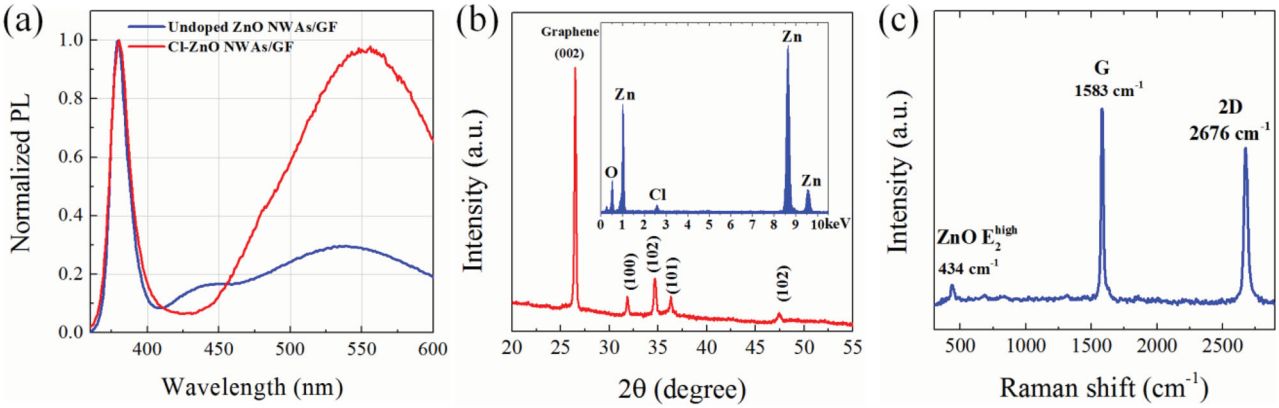

Figure 2. a) Normalized PL spectra of Cl-ZnO NWAs/GF and undoped ZnO NWAs/GF. b) XRD pattern and EDX analysis (inset) of the Cl-ZnO NWAs/GF. c) Raman spectrum of the Cl-ZnO NWAs/GF, the inset shows the diffraction pattern of the ZnO NWAs.

Figure 1c is the schematic illustration of the Cl-ZnO NWAs/GF. Figure 1d–h shows a series of SEM images of the Cl-ZnO NWAs/GF structure. It is clear from Figure 1h that the surface of the GF was fully covered by quasi-vertical aligned Cl-ZnO NWAs. The diameters of the Cl-ZnO nanowires range from 40 to 100 nm. The transmssion electron microscopy (TEM) image in Figure 1i revealed that the surfaces of the Cl-ZnO NWs are rough, which are contrary to the smooth surfaces of undoped ZnO NWs. The rough surfaces on ZnO NWs are usually a strong indication of the existence of high concentration of impurity atoms (point defects), as well as line and planar defects originated in these impurity atoms.[28] It has been demonstrated that a high doping concentration of Cl usually comes with enhanced formation of native defects such as vacancies, which migrate to the surface of ZnO NWs and form surface defects and thus induce rough surfaces.[28] Similar phenomenon has also been observed for ZnO NWs doped with various dopants such as Sb, and Cu.[29–31] The PL measurement results are shown in **Figure 2**a, which compares the normalized PL spectra measured from Cl-ZnO NWAs/GF and undoped ZnO NWAs/GF. From Figure 2a, it is evident that the defect level emission (in the visible region) of Cl-ZnO NWAs/GF is much higher than that of the undoped ZnO NWAs/GF, indicating a higher density of surface defects of the Cl-ZnO NWAs.[32,33] Note that these surface defects often play a very important role in the electronic/chemical properties as well as the oxygen molecule adsorption/desorption behaviors of metal oxides.[34] The X-ray diffraction (XRD) pattern of the Cl-ZnO NWAs/GF is shown in Figure 2b. All the peaks are identified and assigned according to the Joint Committee of Powder Diffraction Standards (JCPDS) data. The GF has a sharp (002) peak centered at $2\theta = 26.4°$. The remaining peaks can be well indexed to the wurtzite ZnO (JCPDS #36-1451) and no impurity phases were observed. The EDX spectrum of the Cl-ZnO NWAs/GF is shown in the inset of Figure 2b. A strong signal of Cl at 2.6 keV is observed, demonstrating the existence of Cl. Further EDX analysis gives a roughly estimated 2.7 at% of Cl with respect to Zn, which suggests a very high doping concentration. A number of NWs are surveyed and the corresponding EDX spectra all gave conspicuous Cl peaks and similar Cl concentration. The Raman spectrum of the 3D GF is shown in Figure 2c. The two prominent peaks near 1580 and 2680 cm^{-1} correspond to the G and 2D bands of graphene. No appreciable D band intensity was observed, which confirmed the overall high quality of the graphene foam.[35] The integrated intensity ratio of the G to 2D band indicates that the walls of the GF are mainly composed of multilayer graphene sheets.[36] In addition to the G and 2D bands for the GF, the peak located near 434 cm^{-1} is the characteristic of ZnO. These results confirm the successful integration of the Cl-ZnO NWAs and the 3D GF.

2.2. Field Emission Characterization

The comparison curves of the current density J verses applied electric field E measured at the same condition (d = 100 μm) from Cl-ZnO NWAs/GF, undoped ZnO NWAs/GF and bare GF are shown in **Figure 3**b. The turn-on fields, defined as the E corresponding to the J of ≈10 μA cm^{-2}, are found to be ≈1.6, ≈2.6 and ≈4.1 V μm^{-1} for Cl-ZnO NWAs/GF, undoped ZnO NWAs/GF, and bare GF, respectively. The threshold fields, defined as the E where J arrives at 0.1 mA cm^{-2}, are found to be ≈2.3, ≈3.3, and ≈5.25 V μm^{-1}, for Cl-ZnO NWAs/GF, undoped ZnO NWAs/GF, and bare GF, respectively. These results demonstrate that the bare GF only contributes to a small portion of the total field emission current of Cl-ZnO NWAs/GF and undoped ZnO NWAs/GF. It can also be observed that the field-emission properties of undoped ZnO NWAs/GF are considerably improved after Cl-doping with much lower turn-on and threshold field. In addition, it can be clearly observed that the current density has been greatly increased from ≈0.41 to ≈1.51 mA cm^{-2} under the same electric field of 4 V μm^{-1} for Cl-ZnO NWAs/GF. The field emission properties of the samples were further analyzed using the Fowler–Nordheim (F–N) theory, which is the most commonly used model for understanding the electron emission from a metal surface under a strong applied field, and it has been also widely used to investigate the electron-emission behavior of various nanostructures, such as CNTs,[37–39] nanowires,[40] and nanowalls.[41] The field-emission characteristics of the Cl-ZnO NWAs/GF and undoped ZnO NWAs/GF were

www.MaterialsViews.com

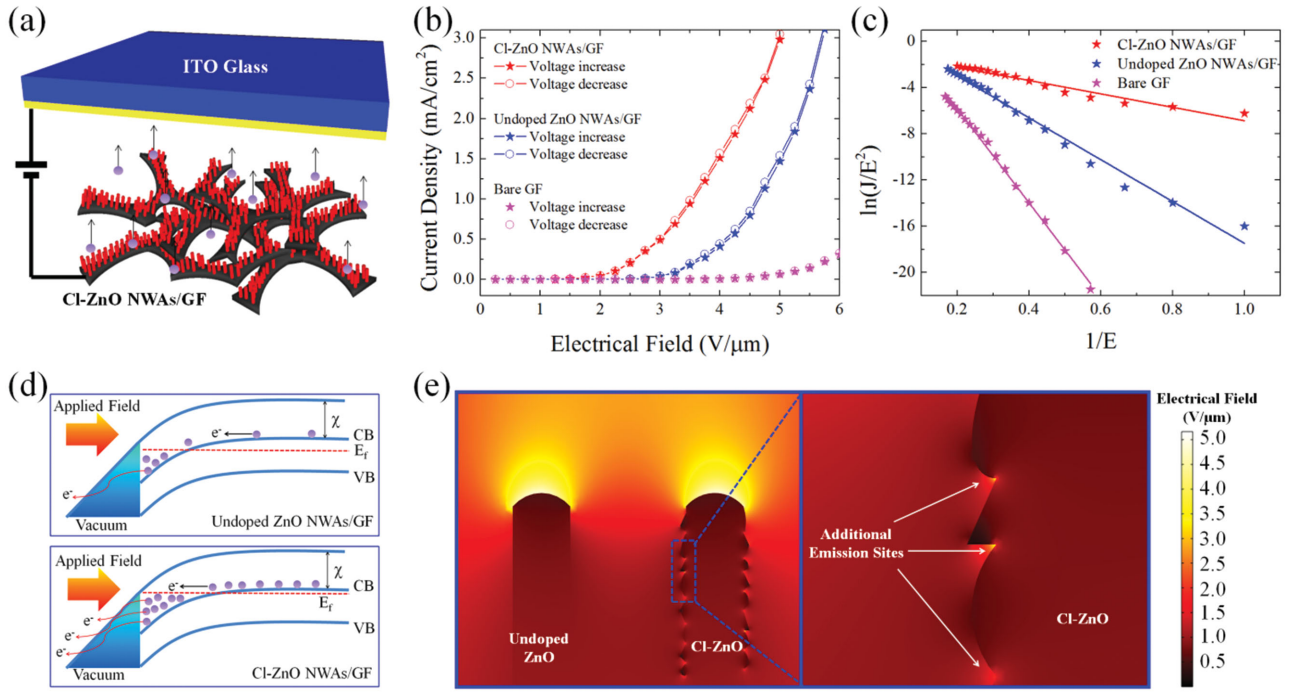

Figure 3. a) Schematic illustration of the field emission measurement setup. b) *J–E* characteristics of Cl-ZnO NWAs/GF, undoped ZnO NWAs/GF, and bare GF during one complete voltage sweeping. c) F–N plots of the corresponding *J–E* curves. d) Schematic energy band diagram of Cl-ZnO NWAs/GF (top panel) and undoped ZnO NWAs/GF (bottom panel). e) 2D electrostatic field simulations of undoped ZnO nanowire and Cl-ZnO nanowire.

further analyzed according to the F–N equation, which is expressed as follows:[42]

$$J = \frac{A\beta^2 E^2}{\phi} \exp\left(-\frac{B\phi^{3/2}}{\beta E}\right) \quad (1)$$

where J is the current density, E is the applied field between the anode and the cathode, A and B are constants ($A = 1.56 \times 10^{-6}$ A V^{-2} eV, $B = 6.83 \times 10^3$ V μm^{-1} eV$^{-3/2}$), ϕ is the work function of the emitter material, and β is the field enhancement factor that reflects the ability of the emitters to enhance the local electric field. The work function of undoped ZnO NWs is around 5.4 eV.[7] If assuming all the Cl dopant (2.7 at% of Cl with respect to Zn) can be ionized at room temperature, the work function of Cl-ZnO is calculated to be around 4.9 eV. Figure 3c is the F–N plots of the relationship between $\ln(J/E^2)$ and $1/E$ for Cl-ZnO NWAs/GF and undoped ZnO NWAs/GF. Interestingly, the F–N plot of the field emission current from both Cl-ZnO NWAs/GF and undoped ZnO NWAs/GF displays a nonlinear relation between $\ln(J/E^2)$ and $1/E$. This nonlinearity can be explained by various mechanisms, including the saturation of conduction current in the ZnO and the nonuniform geometries of the GF. From Figure 3c, the F–N plot of the bare GF showed better linearity as compared to Cl-ZnO NWAs/GF and undoped ZnO NWAs/GF, therefore the nonlinearity of the F–N plots of Cl-ZnO NWAs/GF and undoped ZnO NWAs/GF is mainly determined by the saturation of conduction current in the ZnO. The slope of the F–N plot is equal to $-B\phi^{3/2}/\beta$, from which the value of the field enhancement factor β can be estimated. A number of experiments were performed to ensure the stability and reproducibility. The value of β is found to be around 1430, 4553, and 12844 for bare GF, undoped ZnO NWAs/GF and Cl-ZnO NWAs/GF, respectively. The obtained β of Cl-ZnO NWAs/GF is among the highest as compared to other types of ZnO nanostructure-based field emitters, as shown in **Table 1**. From the literatures in Table 1, we can see that the advantages

Table 1. Field emission characteristics of some ZnO nanostructures recently reported in the literature.

ZnO emitters	Turn-on field [V μm^{-1}]	Enhancement factor (β)	Refs.
In-doped NWs	2.4	9490	[7]
ZnO on reduced graphene oxide	2.1	3150	[14]
In-doped nanochips	2.5	10 640	[42]
Nanorods arrays	2.98	1732	[49]
N-doped nanobullet	2.9	1800	50
Propeller-like	4.36	1294	[51]
In-nanorods	4.7	4660	[52]
Nanoneedles	2.4	1464	[53]
Vertical ZnO NWs on graphene	2.0	6483	[54]
Diamond-coated ZnO nanorods	2.08	4227	[55]
Al-doped ZnO nanowires	1.3	7835	[56]
Ga-doped ZnO nanosheets	4.67	4037	[57]
Mg-doped ZnO nanorods	1.97	4136	[58]
Tetrapod-shaped Sn-doped ZnO	1.95	9556	[59]
Ti-doped ZnO nanoarray	3.2	1970	[60]
ZnO NWAs/GF	2.6	4553	Present work
Cl-ZnO NWAs/GF	1.6	12844	Present work

small NANO MICRO

of using highly conductive graphene-based substrates as a negative electrode for field emitters include can effectively reduce the barrier resistance between the material and the substrate, as well as improved carrier injection and transport efficiency.

The significantly enhanced field emission performance of Cl-ZnO NWAs/GF can be explained as follows: First, the introduction of Cl-dopant in ZnO lifts up the Fermi level of ZnO and hence provides more free electrons in the conduction band of ZnO at room temperature, as shown in Figure 3d. As the electric field established between the Cl-ZnO NWAs/GF and vacuum became larger, greater numbers of electrons moved toward the Cl-ZnO nanowire tips. Second, previous theoretical and experimental studies have demonstrated that surface defects/rough surface can significantly enhance the field emission properties of carbon nanotubes (CNTs), diamond films, graphene fins, and ZnO nanostructures through local enhanced electric field.[43–47] To illustrate this effect, we performed 2D electrostatic field simulations by finite element calculation with COMSOL Multiphysics software. From Figure 3e, it is evident that the rough surface of Cl-ZnO NWAs can significantly enhance the electrical field in certain points along the sidewall of the ZnO Cl-NWAs, therefore resulting in more effective emission sites. Since the Cl-doped ZnO NWAs in this study have a very rough surface due to the high density of surface defects, we believe that these defects also contributed to the enhanced field emission properties of the Cl-ZnO NWAs/GF structure. Third, because of GF's outstanding conductivity, high electron mobility, and a very high specific surface area,[35] using GF as substrate cannot only improve the electron injection efficiency in the interface of GF and ZnO NWAs, but also be able to support a large number Cl-ZnO NWAs as field emission sites.

The cyclic performance of the Cl-ZnO NWAs/GF emitter, over a course of 30 cycles, has been investigated, as shown in **Figure 4**a. The Cl-ZnO NWAs/GF showed extremely stable cyclic performance. The standard deviation of the current across 30 cycles was consistently an order of magnitude less than the measured emission current, highlighting the reproducibility of the emission characteristics. Most importantly, the turn-on voltage does not drift to higher potentials with each cycle, as is often the case for nanocarbon field emitters.[48] This negligible hysteresis, compared to typical nanocarbon field emitters,[48] should be attributed to the high degree of lattice stability during the emission. The long-period emission stability of the Cl-ZnO NWAs/GF was tested by measuring the current density under a constant electric field of 4 V μm^{-1} for over 30 h, as shown in Figure 4b. It can be seen that no obvious degradation of field emission current density was observed during the measurement for both the Cl-ZnO NWAs/GF and undoped ZnO NWAs/GF emitters, with corresponding fluctuation less than 10% and 15%, respectively. These results demonstrate the excellent field emission stability of both Cl-ZnO NWAs/GF and undoped ZnO NWAs/GF.

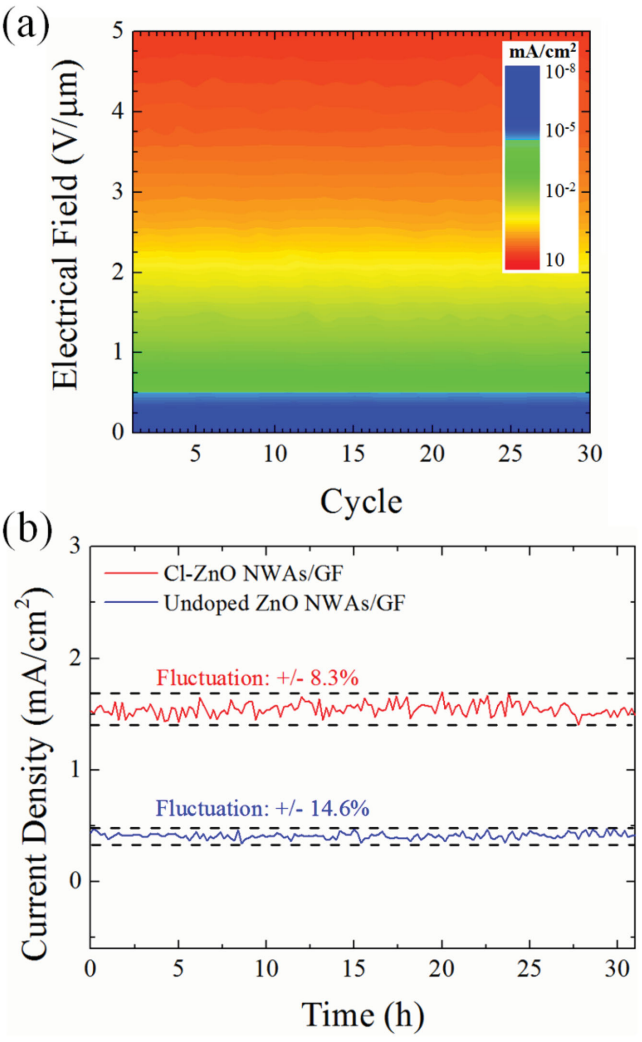

Figure 4. a) Cyclic performance of the Cl-ZnO NWAs/GF. The intensity denotes current density, J (mA/cm). b) Field emission current density as a function of time demonstrates the field-emission stability.

2.3. Photocatalytic Performance Testing

ZnO is a well-known photocatalyst and has been the focus of much attention in the photodegradation and complete mineralization of polluted water. However, most reports have focused on investigating the effectiveness of commercial ZnO or the nanostructured ZnO powder in removing organic compounds from aqueous solutions.[61–63] To utilize these conventional powder photocatalysts, additional separation steps are usually necessary to remove the photocatalysts from the reacting aqueous suspension after the photodegradation process, which is still a major challenge and inevitably increases the cost of the process. Here, the Cl-ZnO NWAs/GF as highly efficient photocatalyst with excellent recyclability was demonstrated, which could help overcome the aforementioned challenges for environment treatment.

The photocatalytic performances of the Cl-ZnO NWAs/GF were evaluated by photodegradation of RhB (a typical organic azo-dye pollutant in the textile industry) in aqueous solution. **Figure 5**a shows the changes of UV–vis spectra and the color of the RhB solutions during the degradation processes. After 75 min, the RhB solution was colorless and the absorption peaks of the RhB solution in both the visible and UV region almost disappeared, indicating the excellent photocatalytic activity of the Cl-ZnO NWAs/GF. For comparison,

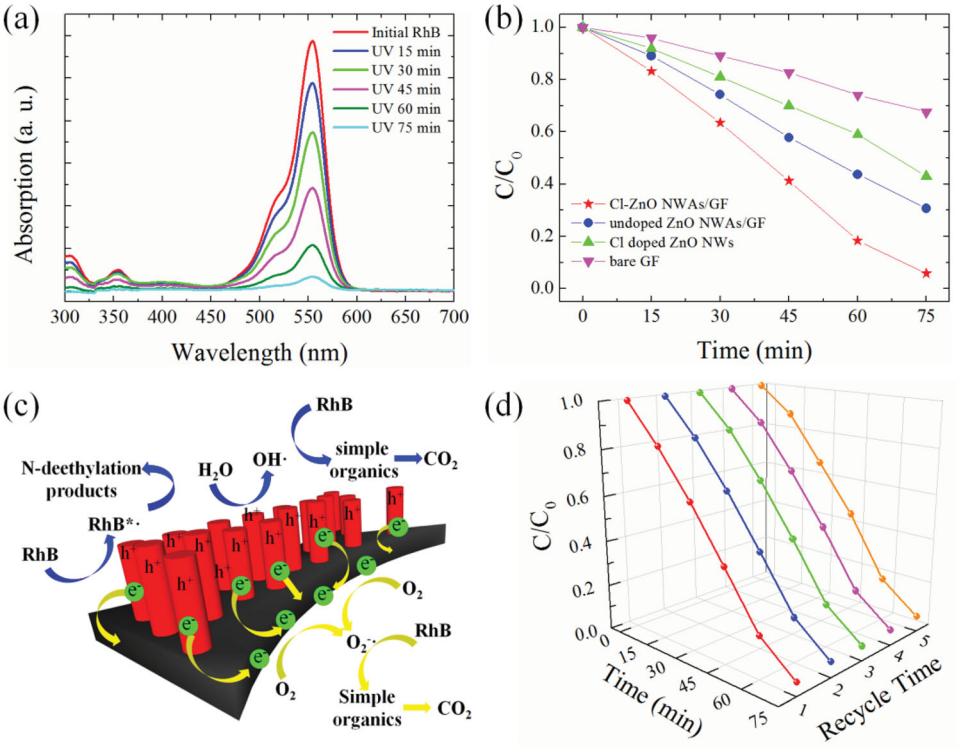

Figure 5. a) UV–Vis absorption spectra change of RhB solution in presence of the Cl-ZnO NWAs/GF under UV irradiation. b) Photocatalytic performance comparison of Cl-ZnO NWAs/GF, undoped ZnO NWAs/GF, Cl-ZnO NWs, and bare GF. c) Schematic illustration of the photocatalytic mechanism of the Cl-ZnO NWAs/GF. d) Recyclable photocatalytic performance of the Cl-ZnO NWAs/GF for the first, second, third, fourth, and fifth cycles.

the photocatalytic performance of an undoped ZnO NWAs/GF, Cl-ZnO NWs (with the same weight of the Cl-ZnO NWAs/GF) and a bare GF were also investigated by comparing the concentration changes of the RhB solution determined by its characteristic absorption peak at 554 nm, as shown in Figure 5b. The photocatalytic degradation efficiency of RhB under UV light follows the order Cl-ZnO NWAs/GF > undoped ZnO NWAs/GF > Cl-ZnO NWs > bare GF.

The intensity decrease of the absorption spectrum of RhB in presence of bare GF is due to the physical adsorption of RhB on the surface of GF. Similar phenomena have also been observed for CNT and graphene.[64–66] The enhancement of photocatalytic activity of Cl-ZnO NWAs/GF is attributed to improved carrier transport and separation efficiency in the material systems, as well as the high density of surface defects on ZnO NWAs introduced by Cl dopant. The schematic illustration of the photocatalytic mechanism of the Cl-ZnO NWAs/GF is presented in Figure 5c. When under UV irradiation, electron-hole pairs are generated in the Cl-ZnO NWAs. The electron affinity for ZnO is 4.2 eV and the work function of the graphene sheet is known to be 4.5 eV below the vacuum level.[67] Thus, when ZnO is in contact with the graphene, it is energetically favorable for the photogenerated electrons to get transferred from the conduction band of ZnO to the graphene, leaving unpaired holes on the ZnO surface. Our recent study[68] and other literatures[69,70] have demonstrated that the surface defects of ZnO nanostructures act as effective hole trapping centers, which can significantly prolong the lifetime of the holes and hence dramatically reduce the recombination probability of photogenerated electron-hole pairs. Consequently, larger number of electrons and holes exist on the active sites of the surface of GF and ZnO NWAs, resulting in enhanced photocatalytic reactions. Since the doping of Cl introduced a high density of surface defects, stronger photocatalytic activity is expected for the Cl-ZnO NWAs/GF as compared to undoped ZnO NWAs/GF. In addition, previous study has demonstrated that Cl dopant can greatly facilitate the electron transport process in ZnO NWs,[21] leading to an improved charge transport and separation efficiency of the Cl-ZnO NWAs/GF as compared to undoped ZnO NWAs/GF. Such an efficient charge transport and separation process provide direct and fast electron/hole transfer to their acceptors (H_2O, O_2, and RhB), leading to a high photodegradation efficiency. Finally, the recyclability of the Cl-ZnO NWAs/GF is tested and the results are shown in Figure 5d. The degradation time of RhB for the fifth cycle is virtually unchanged, demonstrating the excellent recyclability of Cl-ZnO NWAs/GF as a photocatalyst. Previous studies have demonstrated that the photostability of ZnO can be significantly improved by introducing carbon-based nanomaterials including CNTs, Buckminsterfullerene, graphene, and reduced graphene oxide. The improved photostability can be attributed to hybridization interaction between ZnO and these carbon materials, and enhanced physical adsorption ability of organic dyes and enhanced consumption of photogenerated holes from ZnO.[71]

3. Conclusion

We developed an environmentally friendly, low-cost, and large-scale method to synthesize Cl-ZnO NWAs/GF, and investigated its field emission and photocatalytic properties. The introduction of Cl-dopant in ZnO increases free electrons in the conduction band of ZnO and also leads to the rough surface of ZnO NWAs, which greatly improved the field emission properties of the Cl-ZnO NWAs/GF in terms of low turn-on voltage (≈1.6 V μm^{-1}) and high field enhancement factor (≈12844). These results suggest that stable Cl-ZnO NWAs/GF field emitters have great potential for applications such as high-brightness backlighting, flat panel displays, and lighting. Also, the Cl-ZnO NWAs/GF demonstrated a high photocatalytic efficiency under UV irradiation, enabling photodegradation of organic dyes such as RhB within ≈75 min, with excellent recyclability. The excellent photocatalytic performance of the Cl-ZnO NWAs/GF is due to the highly efficient charge separation efficiency at the heterointerface of Cl-ZnO and GF, as well as improved electron transport efficiency in Cl-ZnO NWAs. The results in this work may open up new possibility of using Cl-ZnO and graphene-based hybrid nanostructures for various applications including optoelectronics, photocatalysts, gas sensors, energy storage devices, and biosensors.

4. Experimental Section

Synthesis of Cl-ZnO NWAs/GF: The GF synthesis was performed following the method developed by Hui-Ming Cheng's Group.[36] A scaffold of porous nickel foam is used as a template for growth of GF. Chemical vapor deposition (CVD) is used to deposit carbon atoms on the nickel foam using CH_4 decomposition at 1000 °C under ambient pressure. The sample was then placed in hot HCl solution at 60 °C for 5 h to completely remove the nickel. To maintain the integrity of the GF during the etching process, a thin layer of poly(methyl methacrylate) (PMMA) is also deposited on the surface of the graphene formed on the nickel foam. Finally, free-standing GF was obtained by dissolving the PMMA with hot acetone at 60 °C for 1 h.

Hydrothermal synthesis method was employed to produce the homogeneous vertical Cl-ZnO NWAs on the surface of GF. Initially, 0.01 M $Zn(CH_3COO)_2 \bullet 2H_2O$ was dispersed in methanol. The solution was dropped onto the surface of the GF and was annealed at 200 °C to form a seeding layer of ZnO nanocrystals. A mixed solution consisting of $Zn(NO_3)_2 \bullet 6H_2O$ (50×10^{-3} M), hexamethylenetetramine (HMTA, 50×10^{-3} M), and $AlCl_3$ (5×10^{-3} M), was prepared. Subsequently, the transparent solution was transferred to a Teflon-lined autoclave (Parr, USA) and the graphene foam coated with ZnO thin film was suspended in the solution at 100 °C for 12 h in a regular laboratory oven. Then the growth solution was cooled down to room temperature naturally. The resulting substrate was thoroughly washed with deionized water and absolute ethanol for several times and dried in air at room temperature.

Material Characterization: A Carl Zeiss Ultra 1540 dual-beam SEM was used to determine the morphology of the Cl-ZnO NWAs/GF. The elemental analysis was carried out with energy-dispersive X-ray spectroscopy (EDS) integrated in the SEM. XRD patterns were obtained on an X-ray diffractometer (PANalytical) at room temperature using Cu Kα radiation (λ = 0.15418 nm). The accelerating voltage and the applied current were 40 kV and 80 mA, respectively. Raman spectroscopy was performed using the Renishaw spectrometer with a laser wavelength of 514 nm. Laser average power on the surface of the sample is 100 mW. The photoluminescence (PL) spectra of the samples were measured using a Spex-Fluorolog-Tau-3 spectrofluorimeter with excitation wavelength fixed at 330 nm.

Field Emission Characterization: Field emission measurements of Cl-ZnO NWAs/GF were performed in parallel plate geometry. The vacuum chamber pressure was maintained at 3×10^{-6} Torr during the measurements and all the measurements were carried out at room temperature. The indium tin oxide (ITO) film is coated on glass as an anode and the Cl-ZnO NWAs/GF is deposed on the samples as a cathode. The distance between the top surface of the ZnO/GF to the ITO glass is 100 μm. The voltages are supplied from 1 to 1100 V with the increased step of 25 V to measure emission current using the Keithley 237 high-voltage source-measurement unit.

Photocatalytic Performance Testing: The Cl-ZnO NWAs/GF (2 cm × 2 cm) was immersed into 50 mL RhB solution with a concentration of 5 mg L^{-1}. A 150 W xenon lamp was employed as the UV light source. The distance between the sample and lamp was 10 cm. In order to be able to compare the photocatalysts, the weight of the photocatalysts and the irradiation areas for all the samples was kept the same. The changes of UV–vis spectra for the photodegradation process were measured using Shimadzu UV–vis 2550 spectrophotometer with a deuterium lamp (190–390 nm) and a halogen lamp (280–1100 nm).

Simulation Details: A 2D model under electrostatic module in COMSOL is built; the size of the ZnO nanowires is 100 nm in diameter and 1 μm in length. Relative permittivity of ZnO is set as 8.6. The ZnO nanowires are sandwiched between two aluminum metal plates. The distance between the top metal plates and the top of the ZnO nanowires is 1 μm. The initial electrical potential electric potential of all simulation domains is set to 0. In the simulation, a voltage of 4 V is applied on the top metal plate, and the bottom metal plate is grounded.

Acknowledgements

D.S. acknowledges funding support from the Harris professorship at the Rensselaer Polytechnic Institute. J.L. acknowledges funding support from the USA National Science Foundation (Award: CMMI 1463083). N.K. acknowledges funding support from the USA National Science Foundation (Awards CMMI 1234641 and CMMI 1435783). S.S. acknowledges funding support from the Engineering Research Centers Program of the National Science Foundation under NSF Cooperative Agreement No. EEC-0812056 and in part by New York State under NYSTAR contract C130145.
The affiliation of L. Li was corrected on September 23, 2015.

[1] C.-Y. Chang, F.-C. Tsao, C.-J. Pan, G.-C. Chi, H.-T. Wang, J.-J. Chen, F. Ren, D. P. Norton, S. J. Pearton, K.-H. Chen, L.-C. Chen, *Appl. Phys. Lett.* **2006**, *88*, 173503.

[2] D. C. Look, C. Coskun, B. Clafin, G. C. Farlow, *Phys. Rev. B: Condens. Matter Mater. Phys.* **2003**, *32*, 340.
[3] D. Shao, M. Yu, J. Lian, S Sawyer, *Nanotechnology* **2013**, *24*, 295701.
[4] Z. L. Wang, *J. Phys.: Condens. Matter* **2004**, *16*, R829.
[5] D. Shao, H. Sun, J. Gao, G. Xin, M. A. Aguilar, T. Yao, N. Koratkar, J. Lian, S. Sawyer, *Nanoscale* **2014**, *6*, 13630.
[6] Y. Jin, J. Wang, B. Sun, J. C. Blakesley, N. C. Greenham, *Nano Lett.* **2008**, *8*, 1649.
[7] M. Ahmad, S. Hongyu, J. Zhu, *ACS Appl. Mater. Interfaces* **2011**, *3*, 1299.
[8] N. Pan, H. Xue, M. Yu, X. Cui, X. Wang, J. G. Hou, J. Huang, S. Z. Deng, *Nanotechnology* **2010**, *21*, 225707.
[9] M. Ahmad, C. Pan, W. Yan, J. Zhu, *J. Mater. Sci. Eng. B* **2010**, *174*, 55.
[10] M. Ahmad, J. Zhao, J. Iqbal, W. Miao, L. Xie, R. Mo, J. Zhu, *J. Phys. D: Appl. Phys.* **2009**, *45*, 165406.
[11] Q. Zhao, T. Cai, S. Wang, R. Zhu, Z. Liao, D. Yu, *Appl. Phys. A: Mater. Sci. Process.* **2010**, *100*, 165.
[12] L. Liao, J. C. Li, D. F. Wang, C. Liu, C. S. Liu, Q. Fu, L. X. Fan, *Nanotechnology* **2005**, *16*, 985.
[13] Q. Zhao, S. Q. Feng, Y. W. Zhu, X. Y. Xu, X. Z. Zhang, X. F. Song, J. Xu, L. Chen, D. P. Yu, *Nanotechnology* **2006**, *17*, S351.
[14] R. Zou, G. He, K. Xu, Q. Liu, Z. Zhang, J. Hu, *J. Mater. Chem. A* **2013**, *1*, 8445.
[15] T. S. Sreeprasad, A. A. Rodriguez, J. Colston, A. Graham, E. Shishkin, V. Pallem, V. Berry, *Nano Lett.* **2013**, *13*, 1757.
[16] L. A. Ponomarenko, F. Schedin, M. I. Katsnelson, R. Yang, E. W. Hill, K. S. Novoselov, A. K. Geim, *Science* **2008**, *320*, 356.
[17] N. Petrone, C. R. Dean, I. Meric, A. M. van der Zande, P. Y. Huang, L. Wang, D. Muller, K. L. Shepard, J. Hone, *Nano Lett.* **2012**, *12*, 2751.
[18] M.-Q. Yang, N. Zhang, M. Pagliaro, Y.-J. Xu, *Chem. Soc. Rev.* **2014**, *43*, 8240.
[19] C. Han, Z. Chen, N. Zhang, J. C. Colmenares, Y.-J. Xu, *Adv. Funct. Mater.* **2015**, *25*, 221.
[20] N. Zhang, Y. Zhanga, Y.-J. Xu, *Nanoscale* **2012**, *4*, 5792.
[21] S. Liu, B. Weng, Z.-R. Tang, Y.-J. Xu, *Nanoscale* **2015**, *7*, 861.
[22] Y. Zhang, Z.-R. Tang, X. Fu, Y.-J. Xu, *ACS Nano* **2010**, *4*, 7303.
[23] N. Zhang, M.-Q. Yang, Z.-R. Tang, Y.-J. Xu, *ACS Nano* **2014**, *8*, 623.
[24] S. Liu, M.-Q. Yang, Y.-J. Xu, *J. Mater. Chem. A* **2014**, *2*, 430.
[25] D. Shao, M. Yu, H. Sun, T. Hu, J. Lian, S. Sawyer, *Nanoscale* **2013**, *5*, 3664.
[26] X. Bai, L. Wang, R. Zong, Y. Lv, Y. Sun, Y. Zhu, *Langmuir* **2013**, *29*, 3097.
[27] G. Xie, K. Zhang, B. Guo, Q. Liu, L. Fang, J. R. Gong, *Adv. Mater.* **2013**, *25*, 3820.
[28] F. Wang, J.-H. Seo, Z. Li, A. V. Kvit, Z. Ma, X. Wang, *ACS Appl. Mater. Interfaces* **2014**, *6*, 1288.
[29] F. Wang, J.-H. Seo, D. Bayerl, J. A. Shi, H. Y. Mi, Z. Q. Ma, D. Y. Zhao, Y. C. Shuai, W. D. Zhou, X. Wang, *Nanotechnology* **2011**, *22*, 225602.
[30] A. B. Yankovich, B. Puchala, F. Wang, J. H. Seo, D. Morgan, X. D. Wang, Z. Q. Ma, A. V. Kvit, P. M. Voyles, *Nano Lett.* **2012**, *12*, 1311.
[31] W. Wan, J. Huang, L. Zhu, L. Hu, Z. Wen, L. Sun, Z. Ye, *CrystEngComm* **2013**, *15*, 7887.
[32] J. V. Foreman, H. O. Everitt, J. Yang, J. Liu, *Appl. Phys. Lett.* **2007**, *91*, 011902.
[33] D. Shao, H. Sun, M. Yu, J. Lian, S. Sawyer, *Nano Lett.* **2012**, *12*, 5840.
[34] R. Schaub, E. Wahlstrom, A. Ronnaus, E. Laegsgaard, I. Stensgaard, F. Besenbacher, *Science* **2003**, *299*, 377.
[35] F. Yavari, Z. Chen, A. V. Thomas, W. Ren, H.-M. Cheng, N. Koratkar, *Sci. Rep.* **2011**, *1*, 166.
[36] Z. Chen, W. Ren, L. Gao, B. Liu, S. Pei, H.-M. Cheng, *Nat. Mater.* **2011**, *10*, 424.
[37] W. A. de Heer, J. M. Bonard, K. Fauth, A. Chatelain, L. Forro, D. Ugarte, *Adv. Mater.* **1997**, *9*, 87.
[38] B. Ha, D. H. Shin, J. Park, C. J. Lee, *J. Phys. Chem. C* **2008**, *112*, 430.
[39] K. Y. Chun, C. J. Lee, *J. Phys. Chem. C* **2008**, *112*, 4492.
[40] C. J. Lee, T. J. Lee, S. C. Lyu, Y. Zhang, H. Ruh, H. J. Lee, *Appl. Phys. Lett.* **2002**, *81*, 3648.
[41] T. Yu, Y. W. Zhu, X. J. Xu, Z. X. Shen, P. Chen, C. T. Lim, J. T. L. Thong, C. H. Sow, *Adv. Mater.* **2005**, *17*, 1595.
[42] K. Mahmood, S. B. Park, H. J. Sung, *J. Mater. Chem. A* **2013**, *1*, 8445.
[43] N. A. Fox, W. N. Wang, T. J. Davis, J. W. Steeds, P. W. May, *Appl. Phys. Lett.* **1997**, *71*, 2337.
[44] K. S. Hazra, N. A. Koratkar, D. S. Misra, *Carbon* **2011**, *49*, 4760.
[45] W. Zhu, G. P. Kochanski, S. Jin, L. Seibles, *J. Appl. Phys.* **1995**, *78*, 2707.
[46] T. Hallam, M. T. Cole, W. I. Milne, G. S. Duesberg, *Small* **2014**, *10*, 95.
[47] Q. H. Li, Q. Wan, Y. J. Chen, T. H. Wang, H. B. Jia, D. P. Yu, *Appl. Phys. Lett.* **2004**, *85*, 636.
[48] M. T. Cole, K. Hou, J. H. Warner, J. S. Barnard, K. Ying, Y. Zhang, C. Li, K. B. K. Teo, W. I. Milne, *Diamond Relat. Mater.* **2012**, *23*, 66.
[49] J. H. Lee, Y. W. Chung, M. H. Hon, I. C. Leu, *Appl. Phys. A: Mater. Sci. Process.* **2009**, *97*, 403.
[50] U. K. Gautam, L. S. Panchakarla, B. Dierre, X. Fang, Y. Bando, T. Sekiguchi, A. Govindaraj, D. Golberg, C. N. R. Rao, *Adv. Funct. Mater.* **2009**, *19*, 131.
[51] H. L. Yan, J. B. Wan, X. L. Zhong, *J. Mater. Sci.: Mater. Electron.* **2011**, *22*, 724.
[52] T. H. Fang, S. H. Kang, *Curr. Appl. Phys.* **2010**, *10*, 1076.
[53] Q. Zhao, H. Z. Zhang, Y. W. Zhu, S. Q. Feng, X. C. Sun, J. Xu, D. P. Yua, *Appl. Phys. Lett.* **2005**, *86*, 203115.
[54] J. O. Hwang, D. H. Lee, J. Y. Kim, T. H. Han, B. H. Kim, M. Park, K. No, S. O. Kim, *J. Mater. Chem.* **2011**, *21*, 3432.
[55] K. J. Sankaran, M. Afsal, S.-C. Lou, H.-C. Chen, C. Chen, C.-Y. Lee, L.-J. Chen, N.-H. Tai, I-N. Lin, *Small* **2014**, *10*, 179.
[56] C.-L. Hsu, C.-W. Su, T.-J. Hsueh, *RSC Adv.* **2014**, *4*, 2980.
[57] Y.-H. Liu, S.-J. Young, L.-W. Ji, S.-J. Chang, *IEEE Trans. Electron. Dev.* **2014**, *61*, 4192.
[58] Y.-H. Liu, S.-J. Young, L.-W. Ji, T. H. Meen, C. H. Hsiao, C. S. Huang, S.-J. Chang, *IEEE Trans. Electron. Dev.* **2014**, *61*, 1541.
[59] X. Zhou, T. Lin, Y. Liu, C. Wu, X. Zeng, D. Jiang, Y. Zhang, T. Guo, *ACS Appl. Mater. Interfaces* **2013**, *5*, 10067.
[60] X. Liu, M. Hu, X. Chu, Q. Yan, *J. Mater. Sci.: Mater. Electron.* **2013**, *24*, 2839.
[61] R. Brayner, R. Ferrari-Iliou, N. Brivois, S. Djediat, M. F. Benedetti, F. Fievet, *Nano Lett.* **2006**, *6*, 866.
[62] K. M. Reddy, K. Feris, J. Bell, D. G. Wingett, C. Hanley, A. Punnoose, *Appl. Phys. Lett.* **2007**, *90*, 213902.
[63] C. G. Tian, Q. Zhang, A. P. Wu, M. J. Jiang, Z. L. Liang, B. J. Jiang, H. G. Fu, *Chem. Commun.* **2012**, *48*, 2858.
[64] D. Shao, H. Sun, J. Gao, G. Xin, Ma. A. Aguilar, T. Yao, N. Koratkar, J. Lian, S. Sawyer, *Nanoscale* **2014**, *6*, 13630.
[65] J. H. Im, S. J. Yang, C. H. Yun, C. R. Park, *Nanotechnology* **2012**, *23*, 035604.
[66] J. Lia, S. l. Zhou, G.-B. Hong, C.-T. Chang, *Chem. Eng. J.* **2013**, *219*, 486.
[67] D. Shao, M. Yu, H. Sun, T. Hu, S. Sawyer, *Nanoscale* **2013**, *5*, 3664.
[68] D. Shao, J. Gao, P. Chow, H. Sun, G. Xin, P. Sharma, J. Lian, N. Koratkar, S. Sawyer, *Nano Lett.* **2015**, *15*, 3787.
[69] J. Wang, Q. Li, L. Peng, M. Malac, *Microsc. Microanal.* **2009**, *15*, 1218.
[70] X. Zhang, J. Qin, Y. Xue, P. Yu, B. Zhang, L. Wang, R. Liu, *Sci. Rep.* **2014**, *4*, 4596.
[71] C. Han, M.-Q. Yang, B. Weng, Y.-J. Xu, *Phys. Chem. Chem. Phys.* **2014**, *16*, 16891.

Received: May 18, 2015
Revised: June 4, 2015
Published online: July 16, 2015